Active Control of Irreversible Faradic Reactions to Enhance the Performance of Reverse Electrodialysis for Energy Production from Salinity Gradients

Oh, Yoontaek; Han, Ji Hyung; Kim, Hanki; Jeong, Namjo; Vermaas, David A.; Park, Jin Soo; Chae, Soryong

DOI
10.1021/acs.est.1c02734

Publication date
2021

Document Version
Accepted author manuscript

Published in
Environmental Science and Technology

Citation (APA)
Oh, Y., Han, J. H., Kim, H., Jeong, N., Vermaas, D. A., Park, J. S., & Chae, S. (2021). Active Control of Irreversible Faradic Reactions to Enhance the Performance of Reverse Electrodialysis for Energy Production from Salinity Gradients. *Environmental Science and Technology*, *55*(16), 11388-11396. https://doi.org/10.1021/acs.est.1c02734

Active Control of Irreversible Faradaic Reactions to Enhance Performance of Reverse Electrodialysis for Energy Production from Salinity Gradients

Yoontaek Oh [1], Ji-hyung Han [2], Han-ki Kim [2], Namjo Jeong [2], David A. Vermaas [3], Jin-Soo Park [4,*], and Soryong Chae [1,*]

[1] Department of Chemical and Environmental Engineering, University of Cincinnati, Cincinnati, Ohio 45221, United States

[2] Jeju Global Research Center, Korea Institute of Energy Research, Jeju-si, Jeju Province 63357, Republic of Korea

[3] Department of Chemical Engineering, Faculty of Applied Sciences, Delft University of Technology, 2629HZ, Delft, Netherlands

[4] Department of Green Chemical Engineering, College of Engineering, Sangmyung University, 31 Sangmyungdae-gil, Dongnam-gu, Cheonan-si, Chungnam Province 31066, Republic of Korea

* **Corresponding authors:** Dr. Jin-Soo Park (energy@smu.ac.kr) and Dr. Soryong Chae (chaesg@ucmail.uc.edu)

ABSTRACT

Irreversible faradaic reactions in reverse electrodialysis (RED) are an emerging concern for scale-up, reducing the overall performance of RED and producing environmentally harmful chemical species. Capacitive RED (CRED) has the potential to generate electricity without the necessity of irreversible faradaic reactions. However, there is a critical knowledge gap in the fundamental understanding of the effects of operational stack voltages of CRED on irreversible faradaic reactions and the performance of CRED. This study aims to develop an active control strategy to avoid irreversible faradaic reactions and pH change in CRED, focusing on the effects of a stack voltage (0.9 – 5.0 V) on irreversible faradaic reactions and power generation. Results show that increasing the initial output voltage of CRED by increasing a stack voltage has an insignificant impact on irreversible faradaic reactions, regardless of the stack voltage applied, but a cutoff output voltage of CRED is mainly responsible for controlling irreversible faradaic reactions. The CRED system with eliminating irreversible faradaic reactions, achieved a maximum power density (1.6 W m^{-2}) from synthetic seawater (0.513 M NaCl) and freshwater (0.004 M NaCl). This work suggests that the control of irreversible faradaic reactions in CRED can provide stable power generation using salinity gradients in large-scale operations.

Keywords: capacitive reverse electrodialysis, irreversible faradaic reactions, pH change, salinity gradients, power generation, stack voltage.

Synopsis: Capacitive reverse electrodialysis produces renewable energy from salinity gradients without irreversible faradaic reactions, pH change, and environmentally harmful chemical species.

Graphic for Table of Contents

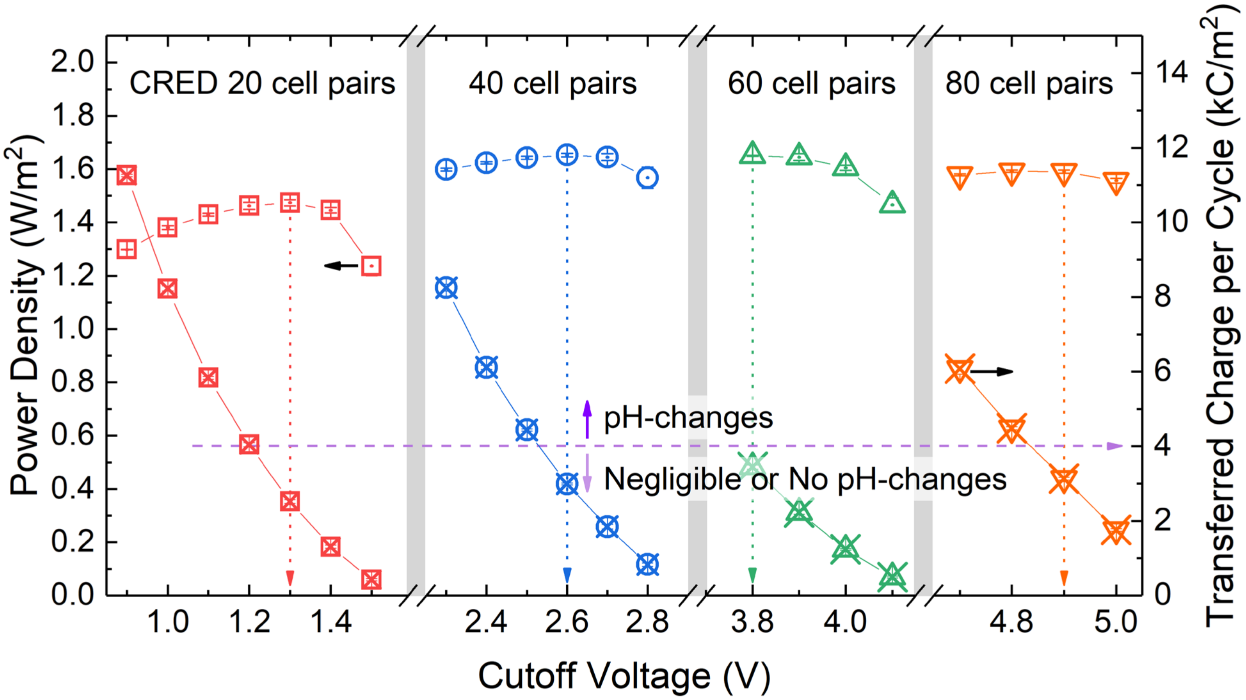

INTRODUCTION

When two aqueous solutions with different salinities are mixed through engineered systems, the salinity gradient can create electric power. One of the most promising energy generation technologies that can harvest electricity from salinity gradients is reverse electrodialysis (RED).[1–3] A RED stack with alternately stacked cation exchange membranes (CEMs) and anion exchange membranes (AEMs) utilizes the chemical potential of the salinity difference between two solutions to create an electrical potential over the membrane. The stack of membrane pairs is sandwiched by a pair of electrodes, where the chemical potential is converted into electricity *via* either reversible or irreversible faradaic reactions. Therefore, in addition to the membrane pairs itself, the electrode systems play a crucial role in power generation with RED.[4–7]

Depending on which faradaic reactions are adopted, electrode systems can be categorized into two groups. The electrode systems adopting irreversible faradaic reactions and electrolytes could generate toxic gas (*e.g.*, Cl_2) and explosive gas (*e.g.*, H_2).[8–10] The gas-evolution processes, mainly caused by water electrolysis, consume significant energy, ultimately reducing RED's net power generation.[4,11,12] Moreover, diffusion of chloride ion (Cl^-) towards the electrode rinse solution is inevitable, as shielding membranes are never perfectly selective, implying the electrode rinse solution (ERS) needs to be purified frequently to avoid chlorine evolution. The other electrode systems adopting reversible faradaic reactions utilize either reactive electrodes (*e.g.*, Cu or Zn) or inert electrodes with homogeneous redox couples (*e.g.*, $Fe^{2+/3+}$ or $Fe(CN)_6^{3-/4-}$).[1,4,5,7,9] One of the main advantages of these electrode systems is that the overall chemical reaction is null, which consumes much lower energy than irreversible faradaic reactions during redox reactions.

In RED, inert electrodes with homogeneous redox couples are more favorable than reactive electrodes due to the better energy efficiency and the more straightforward design of the stack.[4,5,7] However, they also face operational limitations.[13] For example, $Fe(CN)_6^{3-/4-}$ can be decomposed into cyanide (a highly toxic chemical compound) under sunlight and oxygen or acidic conditions (at accidental overcharging), and $Fe^{2+/3+}$ can form precipitations above pH 2 – 3.[4,6,11,14] Moreover, some inert electrodes, for instance, platinum-coated electrodes, are rather expensive but not proper for irreversible faradaic reactions in electrode systems.[4]

Although a RED system adopts a redox couple, it can still generate harmful gases from irreversible faradaic reactions when operated at a high stack voltage. Han et al. (2019) reported that gas evolution took place continuously in the pilot-scale RED system with a pair of inert electrodes and $Fe(CN)_6^{3-/4-}$ redox couple due to water electrolysis.[12] This phenomenon took place because the concentration polarization of the redox couple easily occurs locally in large stacks with high stack voltages, which leads to large (local) overpotentials for the $Fe(CN)_6^{3-/4-}$ redox couple, exceeding the minimum potential of water electrolysis (*i.e.*, theoretically 1.23 V as standard electrode potential). Blue precipitation was also observed at the anode where oxidation reactions took place, indicating that ferricyanide ($Fe(CN)_6^{3-}$) was decomposed due to the abrupt pH changes caused by water electrolysis.[12]

In contrast, Nam et al. (2019) deliberately employed water electrolysis for the RED system with 1,000 cell pairs to reduce costs and eliminate environmental impacts from using chemicals, such as redox couples. [15] However, water electrolysis caused undesirable inorganic fouling by magnesium hydroxide and calcium carbonate precipitates on the cathode due to the excessive presence of hydroxide ions (OH^-), leading to a decrease in the RED performance. Therefore, it is paramount to adopt a proper electrode system for RED that maintains the performance while mitigating the environmental impacts at the high stack voltage.

There is an alternative engineered system using cost-effective and sustainable electrode systems. Capacitive mixing (CapMix) adopts capacitive electrodes. In CapMix, an externally applied electric potential charges the electrodes immersed in a highly concentrated solution with opposite ions. When the external potential is replaced with external load, and the high concentration solution is switched to a low concentration solution, the accumulated ions are discharged from the electrodes, producing electrical power.[16,17] CapMix equipped with ion exchange membranes (IEMs) enables charging and discharging of the electrodes without the external potential, which showed improved performance; however, the achieved power density was limited at 0.007 – 0.2 W m^{-2}.[18,19]

A new concept process has been developed to address the challenges associated with RED and CapMix systems (*i.e.*, the environmental concerns and low power density). For example, Vermaas et al. (2013)[20] developed a capacitive RED (CRED) process by integrating RED and CapMix with activated carbon capacitive electrodes but without the use of redox couples that showed 0.95 W m^{-2} at 3 – 4 V from synthetic seawater (0.508 M NaCl), freshwater (0.017 M NaCl), and electrolyte (0.25 M NaCl).[20]

The use of capacitive electrodes has been successfully demonstrated for several other electrochemical membrane technologies, including desalination and energy generation technologies.[13,21] However, the performance of the capacitive electrode system has been constrained by relatively small-scale membrane cell pairs at a low stack voltage than the previous study[20], which leads to a poor understanding of a scaled-up capacitive electrode system at a high stack voltage that is much higher than that needed for water electrolysis to occur. Since the current density and corresponding electrode overpotential determine the range of practical operation for the CRED technology, the study of the performance behavior of the scaled-up CRED can provide insight into the optimal operating conditions of the system and the potential for an alternative RED configuration.

This study aims to develop an active control strategy of CRED to avoid irreversible faradaic reactions, focusing on the effects of stack voltage of the CRED system on pH change and power generation in an advanced CRED stack. While the voltage drop between the electrode and ERS determines irreversible faradaic reactions, including water electrolysis, the stack voltage is adopted as a practical approach to control irreversible faradaic reactions and pH.

The constant load (CL) discharge technique that facilitates continuous power generation is applied to figure out the critical factors, such as cutoff voltages (*i.e.*, the voltage where the feed solutions are switched) and the number of cell pairs, which influences the CRED performance. Finally, the maximum power density obtained with different cell pairs in a bench-scale CRED is compared with a conventional RED.

MATERIALS AND METHODS

A Bench-scale CRED and RED. Figure 1 shows a schematic diagram of a bench-scale CRED system. The system is composed of AEMs, CEMs, polytetrafluoroethylene (PTFE) gaskets (0.1 mm thickness) and spacers (0.1 mm thickness) between the membranes, and a pair of activated carbon (AC) capacitive electrodes (Sion Tech Co., South Korea) at the end compartments. The AC loading of the electrode is approximately 9 mg cm^{-2}. The projected area of the electrode was 19.6 cm^2 (5 cm in diameter). All electrodes were immersed in 0.513 M NaCl (Fisher Scientific) solution under vacuum for 4 hours before use in the CRED system. The CRED system with various cell pairs (20 – 80 cell pairs) of CEM (CEM-Type I, FUJIFILM Manufacturing Europe B.V.) and AEM (AEM-Type I, FUJIFILM Manufacturing Europe B.V.) was tested. The membranes were stored in 0.513 M NaCl solution at 4 °C before use. Each cell pair has an effective area of 39.3 cm^2.

Synthetic high concentration (HC) (0.513 M NaCl) and low concentration (LC) (0.004 M NaCl) solutions were prepared by dissolving NaCl in deionized water (1 – 2 μS cm^{-1}). The initial conductivity of the HC and LC solutions were 48.5± 0.1 mS cm^{-1} and 500 ± 5 μS cm^{-1} at room temperature (22 ± 1 °C), respectively. Note that the conductivity of LC represents river water conductivity.[22] The initial pH of the HC and LC feed solutions were 6.0 ± 0.1 and 5.7 ± 0.1, respectively. The same composition of HC solution was also used as ERS.

Two feed solutions were fed into feed solution compartments at 5 mL min^{-1} per compartment using a peristaltic pump (Cole-Parmer). The ERS was fed into the electrode compartments at 5 mL min^{-1} per compartment using a peristaltic pump while the circuit was opened. It usually took less than one minute to obtain a stable voltage of the system (data not shown). Once stabilized, an external resistor was connected, and the system started discharging. When the voltage decreased below cutoff, the feed solutions were switched, which completed a half-cycle. The experiments repeated at least four cycles (*i.e.*, eight half-cycles) unless stated otherwise. Still, results are shown excluding the first cycle as the system showed a stable and reliable voltage profile after the first cycle.

A conventional RED system is the same as the CRED system, except for the electrodes and the ERS. A bench-scale conventional RED system with platinum-coated titanium mesh electrodes (5 cm diameter, Wesco Electrode, South Korea) was tested in this study. A mixed solution that consists of 0.05 M potassium ferricyanide ($K_3[Fe(CN)_6]$), 0.05 M potassium ferrocyanide ($K_4[Fe(CN)_6]$), and 0.1 M sodium sulfate (Na_2SO_4) (Junsei Chemical Co.) was used as the ERS and fed into the system at 50 mL min^{-1} using a peristaltic pump. The conventional RED details can be found in our previous study.[23]

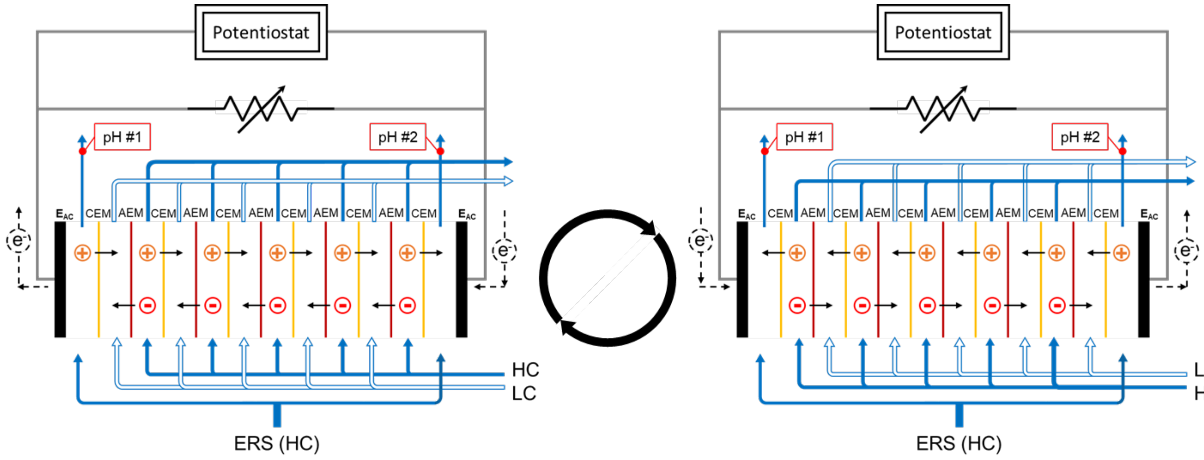

Figure 1. Schematic diagram of a bench-scale CRED system and operating sequences. The system consists of multiple cell pairs (5 cell pairs in this diagram) and a pair of activated carbon electrodes (E_{AC}). Each cell pair consists of a CEM and an AEM. HC and LC solutions flow through the channels alternately and are switched periodically. The potentiostat measures the voltage of the system.

Characterization of AC Electrodes and Membranes. Scanning electron microscope (SEM) coupled with energy-dispersive X-ray spectroscopy (EDX) (Scios DualBeam, Thermo fisher scientific) characterized surface morphology and structure of the AC electrode and membranes. Specific surface area, average pore diameter, and cumulative pore volume of the AC electrode were measured and calculated based on the Brunauer-Emmett-Teller (BET) method (ASAP 2060, Micromeritics) with nitrogen as the analysis adsorptive at 77 K. The sample was dried overnight and degassed using nitrogen gas at 200 °C to remove moisture in the sample.

The electrochemical characterization of the AC electrode was performed using a potentiostat (SP-150, BioLogic) with a three-electrode system in 1 M KCl (Sigma-Aldrich) aqueous electrolyte. The working electrode, the counter electrode, and the reference electrode were the AC electrode, platinum gauze (52 mesh, MilliporeSigma), and Ag/AgCl electrode (BioLogic), respectively. The cyclic voltammetry (CV) curve was obtained at 5 mV s^{-1} under the potential window of -0.5 V through +0.5 V. Galvanostatic charge/discharge cycles were performed at 0.25, 0.5, and 1 A g^{-1} under the same potential window.

Assessment of CRED and RED Performance. In this study, the CL discharge technique was adopted to assess the CRED performance, eliminating an intermittent current interrupt time and continuously producing energy. The CRED system was connected to the potentiostat that measured voltage and an external resistor that produced energy in parallel. Using the resistance and its voltage, the average power and the average power density can be calculated using the following equations[20,24]

$$P = \frac{1}{t - t_0} \sum \frac{\Delta E^2}{R_{ext}} \times \Delta t \quad (1)$$

$$P_{\mathrm{d}} = \frac{P}{N_{\mathrm{cell}} A_{cell}} \quad (2)$$

where P is the average power from the CRED system-generated per cycle (W), t_0 and t are the time in the beginning and the end of the cycle (second), ΔE is the voltage of the resistors, which is the same for the CRED system, R_{ext} is the external resistance (Ω), Δt is the time interval of the voltage measurement during the process, which was one second for the current study, P_{d} is the average power density per cycle (W m^{-2}), N_{cell} is the number of cell pairs (-), and A_{cell} is the effective membrane area of a single cell pair (m^2).

Similarly, the average amount of transferred charge per unit projected electrode area through the external resistance per cycle was calculated using the following equation.

$$Q_d = \frac{1}{A_{ele}} \frac{1}{t - t_0} \sum \Delta I \times \Delta t \qquad (3)$$

where Q_d is the average transferred charge per unit projected electrode area through the external resistor per cycle (C m^{-2}), A_{ele} is the projected electrode area of an electrode (m^2), and ΔI is the current flowing through the resistors (A). The pH variation at the cathode and anode of the system was monitored by measuring the solution pH of the ERS effluents from the cathode and anode, respectively.

The performance of the CRED system was compared to that of the conventional RED system with the CL discharge technique. In addition, to verify the validity of the CL discharge technique, the RED performance is evaluated and compared using two other electrochemical techniques: linear sweep voltammetry (LSV) and constant current (CC) chronopotentiometry (Figure S2).

RESULTS AND DISCUSSION

Characteristics of AC Electrodes for CRED. The AC electrode exhibited well-distributed fine AC particles in contact with the graphite sheet current collector with an activated carbon layer thickness of 150 μm (Figure S3). The BET surface area and average pore size are 1173 m^2 g^{-1} and 2.1 nm, respectively (Figure S4). The electrode is quite hydrophilic and good electrode material for the liquid electrolyte (Figure S5).

The electrochemical properties of the AC electrode were evaluated using CV and galvanostatic charge/discharge tests. Figure 2A shows the CV curve of the AC electrode at a fixed scan rate of 5 mV s^{-1}. The AC electrode exhibits a quasi-rectangular CV profile without conspicuous gas evolution during the measurement, demonstrating the typical behavior of an electric double-layer capacitor. Figure 2B shows the galvanostatic charge/discharge curves of the AC electrode with various current densities (0.25 – 1 A g^{-1}). The specific capacitance was determined using the following equation.

$$C_s = \frac{I \Delta t}{\Delta V m} \qquad (4)$$

where C_s is the specific capacitance (F g^{-1}), I is the discharge current (A), Δt is the discharge time (second), ΔV is the potential change during discharge (V), and m is the weight of the AC loading on the electrode (g). The symmetric charge/discharge characteristic for the AC electrode demonstrates the typical triangular shape of ideal double-layer capacitor behavior. The specific capacitance of the AC electrode was 67.75 F g^{-1} (= 0.610 F cm^{-2}) at 0.25 A g^{-1}, 57.5 F g^{-1} (= 0.518 F cm^{-2}) at 0.5 A g^{-1}, 42 F g^{-1} (= 0.378 F cm^{-2}) at 1 A g^{-1}, respectively. At the beginning of the discharge curve at different discharge currents, the IR drop showed the AC electrode internal resistance of 2.17 Ω.

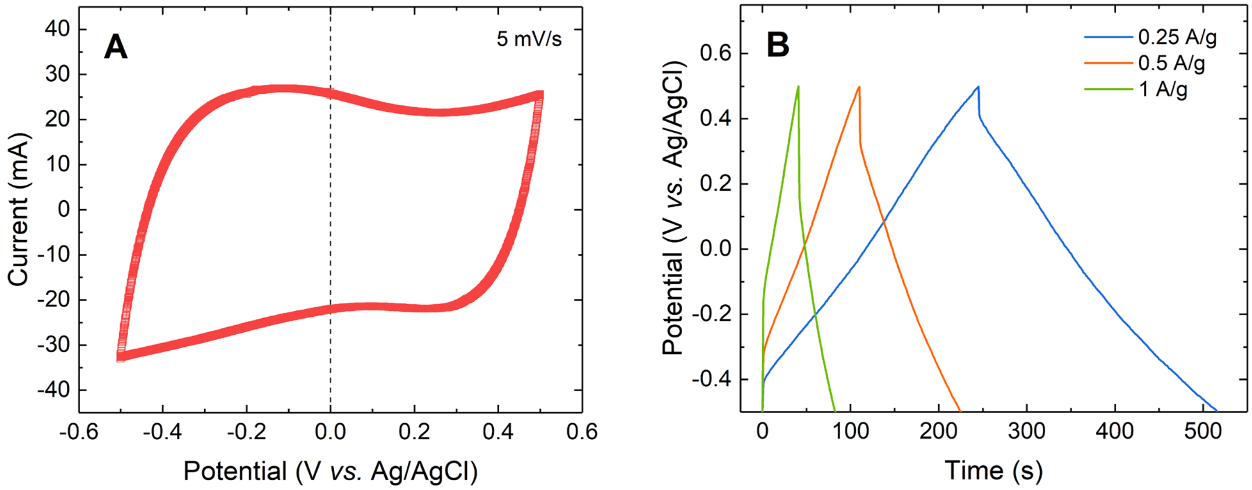

Figure 2. Electrochemical characterization showing CV curve at a scan rate of 5 mV s^{-1} (A) and galvanostatic charge/discharge at different current densities ranging from 0.25 to 1 A g^{-1} (B) in 1 M KCl electrolyte solution.

Power Generation of RED. The performance of a conventional RED system consisting of 20 cell pairs was evaluated using the CL discharge technique (Figure 3). Various external resistors (14 – 26.4 Ω) with approximately 2 Ω increments were tested to find an external resistance that gave the maximum power density of the system. Each external resistor was connected to the RED system, and the voltage was logged. The power density from the CL discharge technique was calculated using the following equation and Eq. 2.

$$P = \frac{\Delta E^2}{R_{ext}} \tag{5}$$

The maximum power density of 1.69 W m^{-2} was obtained with the connected external resistors at 16.1, 18.2, and 20 Ω, respectively. The operating voltage changed with connected external resistors (*i.e.*, increased with higher external resistances). Although it could be possible to obtain a little higher power density between 16.1 and 18.2 Ω or between 18.2 and 20 Ω, this would not differ significantly from the present result.

Based on the results, the external resistor of 18.2 Ω was selected as a representative external resistor that gave the maximum power density of the RED system with 20 cell pairs. The operating voltage was 1.56 V when the 18.2 Ω resistor was connected to the RED system. The same procedure was applied to the RED system at different numbers of cell pairs (Table S1).

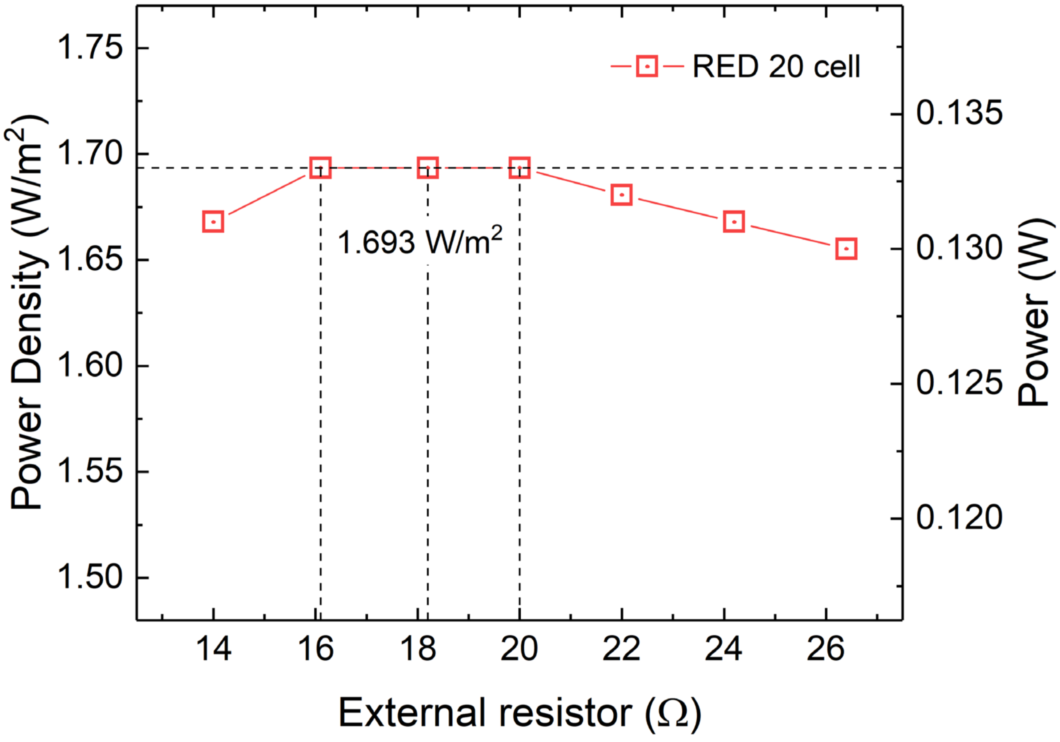

Figure 3. The power density of the conventional RED system consisting of 20 cell pairs obtained from constant load (CL) discharge with different external resistors.

Effect of cutoff voltage on irreversible faradaic reactions and CRED performance. Figure 4A shows voltage and power profiles of the CRED system consisting of 20 cell pairs connected to an external resistor of 18.2 Ω at different cutoff voltages. The test was done between 0.9 – 1.5 V with a 0.1 V difference, but only the selected data are shown. The different cutoff voltages resulted in the changes in each cycle's maximum voltage, discharge time, and average power density. The lower cutoff voltage led to a longer discharge time because the electrode discharged more ions, and therefore a larger fraction of the available capacity was utilized.[24] Also, the cutoff voltage determined the maximum voltage in the following half-cycle. The difference between the cutoff voltage and the maximum voltage in the following half-cycle was found to be around 3.0 V for all cutoff voltages.

Therefore, ± 1.5 V was essentially the highest cutoff voltage, resulting in a symmetric voltage profile for the current system setup. Moreover, the highest cutoff voltage was close to the operating voltage obtained from the conventional RED system (1.56 V) under identical experimental conditions (20 cell pairs connected to 18.2 Ω). Similarly, the highest cutoff voltage for the CRED system with 40, 60, and 80 cell pairs was 2.8, 4.1, and 5.0 V, respectively, each of which is close to the operating voltages obtained from the conventional RED system under identical experimental conditions (i.e., 2.85, 4.05, and 5.10 V, respectively).

This relation originates from swapping the HC and LC fluids, which reverses the potential difference over the RED membrane pairs. The total CRED stack voltage can be decomposed in a RED voltage (V_{RED}), provided by the membrane pairs, and a capacitive potential at switching ($V_{\mathrm{C,switch}}$) due to charge accumulation at the electrodes. Upon switching, the HC and LC fluids, the V_{RED} switches to $-V_{\mathrm{RED}}$, while the sign of $V_{\mathrm{C,switch}}$ remains the same. It can be described as switching at a cutoff voltage $V_{cutoff} = V_{RED} + V_{C,switch}$ to opposite membrane potential, so $V_{max} = -V_{RED} + V_{C,swtich}$, in which V_{max} is the highest voltage obtained at the start of the new half-cycle in CRED (V). Combining these two equations yields the highest cutoff voltage of the current CRED system for a symmetric voltage profile, as a function of the operating voltage acquired from the conventional RED:

$$V_{cutoff} = 2V_{RED} + V_{max} \tag{6}$$

Please note that V_{max} always has an opposite sign compared to V_{cutoff}, $|V_{max}| \geq |V_{cutoff}|$, and V_{REl} which allows writing this as:

$$|V_{cutoff}| = 2V_{RED} - |V_{max}| \tag{7}$$

For the minimum cutoff voltage, side reactions need to be considered. The previous study by Vermaas et al. (2013)[20] reported that each half-cycle's voltage profile in the CRED process decreased linearly with a short switching interval (8 minutes). In contrast, the non-linear voltage profile was exhibited at the end of each half-cycle when a switching interval (*i.e.*, discharge time) was prolonged (33 minutes).[20] Note this previous study[20] adopted CC chronopotentiometry. The authors detected that the non-linear voltage profile and the pH changes appeared when the difference between the stack voltage (U_{CRED}) and the membrane voltage (U_{mem}) exceeds 0.9 V. U_{CRED} represents the overall CRED stack voltage that decreases with time because the system discharges. On the contrary, U_{mem}, representing the sum of the voltage over the membrane cells under given conditions, is constant because of the consistent salinity gradient maintained between two solutions and operating conditions in CRED.

Similar but different trends were observed for the current CRED system with the CL discharge technique (Figure 4A and B). Since the lower cutoff voltage led to the larger amount of charge transferred, the lower cutoff voltage and, therefore, longer discharge time resulted in larger changes in pH. There are two distinct differences between the current study and the previous study.[20] First, in this study, the linearity of the voltage profile is inapplicable to determine whether the pH changes occur because when the capacitive electrode discharges through a constant resistor, the voltage drops exponentially. Second, the pH changes start from the cutoff voltage of 1.2 V (U_{CRED}), which is only about 0.36 V lower than the operating voltage 1.56 V (U_{mem}) from RED connected to 18.2 Ω and is much less than 0.9 V from the previous study.[20] Moreover, as depicted in Figure 4C, when pH started fluctuating, approximately 4 kC m^{-2} of the charge transferred. The fluctuation became exacerbated when lowering the cutoff voltages, which means that irreversible faradaic reactions occurred on both electrode compartments. When the cutoff voltage was 0.9 V, approximately 11.2 kC m^{-2} of the charge transferred, the pH of effluent from the cathode increased to 10.1, and the pH of effluent from the anode decreased to 3.6.

Recent studies on pH changes induced by high overvoltages in capacitive electrodes revealed that this significant fluctuation in pH is attributed to irreversible faradaic reactions, including water oxidation and reduction that generate H^+ and OH^-, respectively, and conceivably other irreversible faradaic reactions, such as hydrogen peroxide (H_2O_2) generation and subsequent consumption that contribute to the pH changes in capacitive electrochemical systems.[25–29] However, it is complicated to distinguish which reactions are more favorable than the others during the operation.

In addition, it was assumed that given the high concentration (0.513 M of NaCl) of ERS and the range of the pH changes (i.e., pH 3.5 – 10), the AC electrode performance was not influenced by the pH changes capacitance (mobility ratio H^+/Na^+ is about 6.9 and OH^-/Cl^- is about 2.6).[27] Isolating the effect of pH on electrode performance would require a completely different study, which is complex and beyond the scope of this study. Despite the complexity, it is obvious that the CRED power performance decreases with the occurring pH changes.

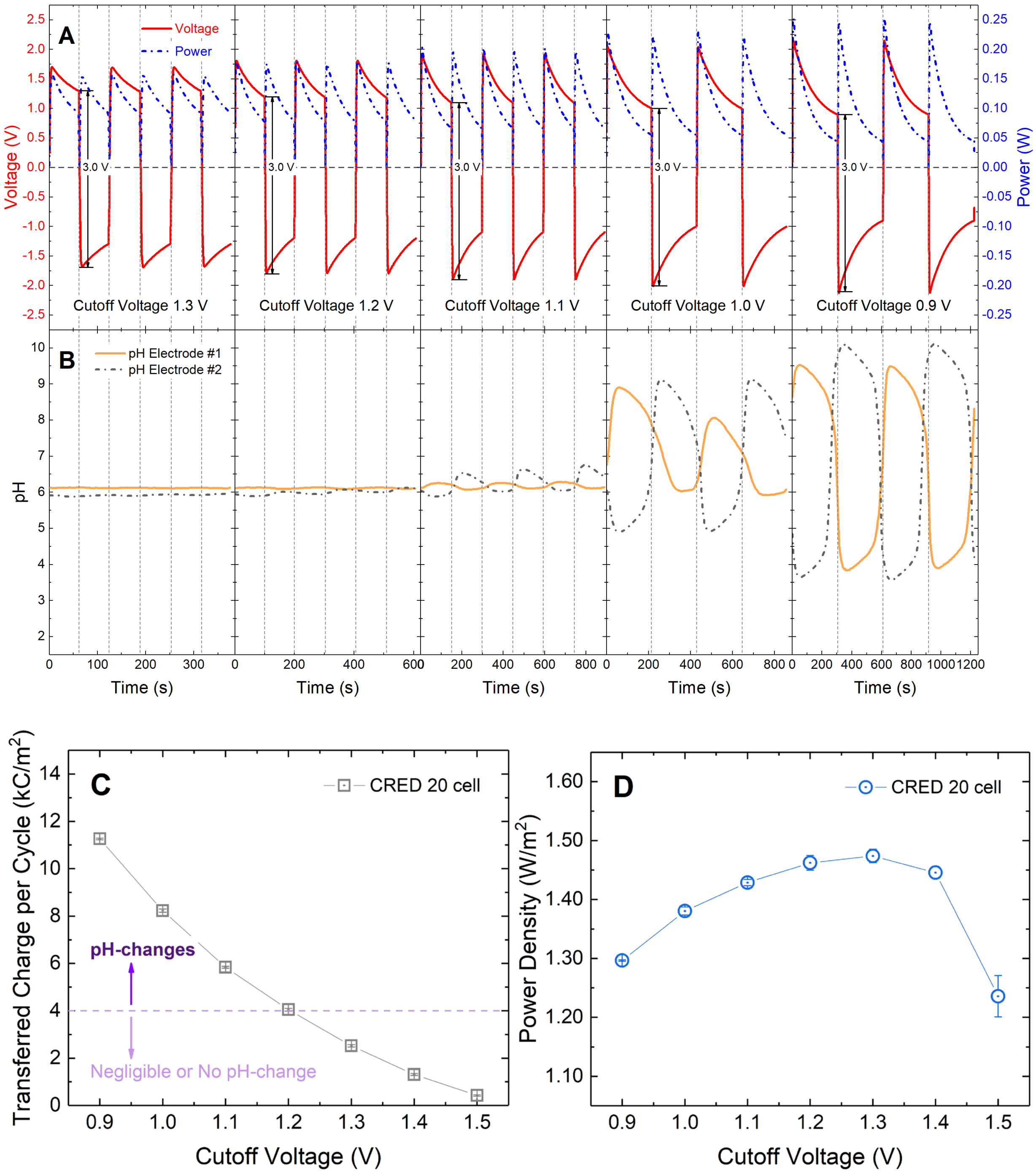

Figure 4. The voltage and corresponding power profile (A) and the pH changes of the bench-scale CRED system with 20 cell pairs connected to an external resistor (18.2 Ω) between 0.9 – 1.5 V cutoff voltages (B), transferred charge per cycle (C), and the power densities at different cutoff voltages (D).

Figure 4D shows the overall power density of the CRED system with 20 cell pairs at the different cutoff voltages. The power densities were increased from the cutoff voltages 1.5 to 1.3 V then started decreasing, most likely due to irreversible faradaic reactions that consume energy generated from the salinity gradient. Despite the earlier onset of pH changes in the electrode compartments, the power density is much higher than for previous CRED work[20], thanks to optimized RED cells (lower resistances, higher salinity gradient) and fast switching (which allows reducing the OCV interval between the switching). The detailed power profiles and the average power densities are shown in Figure S6. The cutoff voltage of 1.5 V shows the extreme of switching very frequently, which yields a lower power density than when using a cutoff voltage of 1.3 V, revealing an inherent limitation of the CRED system; the necessity of a periodic switching of the feed solutions to regenerate the electrodes.

The switching of feed solutions reverses the voltage polarity and the current direction, resulting in the sudden drop in power generation during the switching period. For example, one full cycle at 1.5 V cutoff voltage takes only approximately 24 seconds, including the switching period of approximately 8 – 9 seconds (Figure S6A). More than 30% of the time per cycle for switching causes a decrease in average power and power density.

On the other hand, the cutoff voltage of 0.9 V with a much longer discharge time and much higher peak power than the other cutoff voltages also show a lower power density than 1.3 V (Figure S6D). The prolonged discharge time due to irreversible faradaic reactions decreased the overall average power and the power density. It is noteworthy that although the slight pH changes do not considerably decrease the performance of the system (*e.g.*, the power density at 1.1 V cutoff voltage), the performance decline starts with the pH changes in the electrode system.

Therefore, it is paramount to set cutoff voltage as low as possible unless the pH changes occur to obtain a maximum power density. Together with the practical need for an indicator of the system to maximize power generation, this result demonstrates that the CRED process can generate sustainable and comparable power without significant pH changes.

Effect of Number of Cell Pairs. The CRED system with 40, 60, and 80 cell pairs was connected to external resistors of 30.1, 41.8, and 51.9 Ω, respectively. The maximum power densities of 40, 60, and 80 cell pairs are 1.65 ± 0.01 W m^{-2} at 2.6 V, 1.65 ± 0.00 W m^{-2} at 3.8 V, and 1.59 ± 0.01 W m^{-2} at 4.9 V cutoff voltage, respectively (Figure 5A). Apparently, the maximum power density is obtained at the lowest cutoff voltage without the pH changes, which is a similar trend of 20 cell pairs. The voltage differences between the operating voltage (U_{mem}) and the cutoff voltage (U_{CRED}) where the pH changes start are 0.35, 0.35, and 0.3 V, respectively, which is consistent with the result of 20 cell pairs. For 80 cell pairs, the power density at the cutoff voltage of 4.8 V (1.59 ± 0.00 W m^{-2}) is marginally higher than 4.9 V, but this accompanies the pH changes. It is obvious that the lower the cutoff voltage applies, the more significant pH changes occur, which leads to a decrease in the power density.

As shown in Figure 5B, the pH changes for all cell pairs correlate with the amount of charge transferred strongly during discharge (Figure 5B). In this study, the pH changes started with the amount of transferred charge over approximately 4 kC m^{-2} regardless of the number of cell pairs, which is much lower than the reported value (*i.e.*, 20 kC m^{-2}) from Vermaas et al. (2013).[20] The difference is most likely due to the specific capacitance or total capacitance of an electrode. The previous study[20] used the high-performance capacitive electrode showing the specific capacitance of 1.2 F cm^{-2} (or total electrode capacitance of 120 F). In contrast, the current study used the electrode that showed only 0.52 F cm^{-2} (or total electrode capacitance of 10 F). Note that all discharge currents of CRED for maximum power density are in a range of approximately 80 – 100 mA, which is close to the current density of 0.5 A g^{-1} (88.4 mA) in galvanostatic charge/discharge.

A higher areal-specific capacitance means that a larger quantity of charge can be stored in the same projected electrode area. Thus, it appears that a relatively sufficient charge in the same area is more capable of prohibiting irreversible faradaic reactions. Consequently, the voltage where the pH changes occur may vary and rather depends on the electrode characteristics, such as the specific capacitance or total capacitance.

Therefore, from the consistent results of the voltage difference and the amount of transferred charge, it can be concluded that the pH changes in CRED depend on the electrode properties. Moreover, a longer discharge time per cycle could be achieved by increasing the specific capacitance of electrodes since a higher capacitance takes longer to discharge under identical conditions. The average time per cycle for 20, 40, 60, and 80 cell pairs when the maximum power density is obtained is 125, 127, 141, and 126 seconds, respectively; this means approximately every minute, feed solutions need to be switched. It could be an issue in the context of the cost for frequent solution switching. In other words, extending the discharge time while maintaining the performance should be considered in actual facility-scale operations.

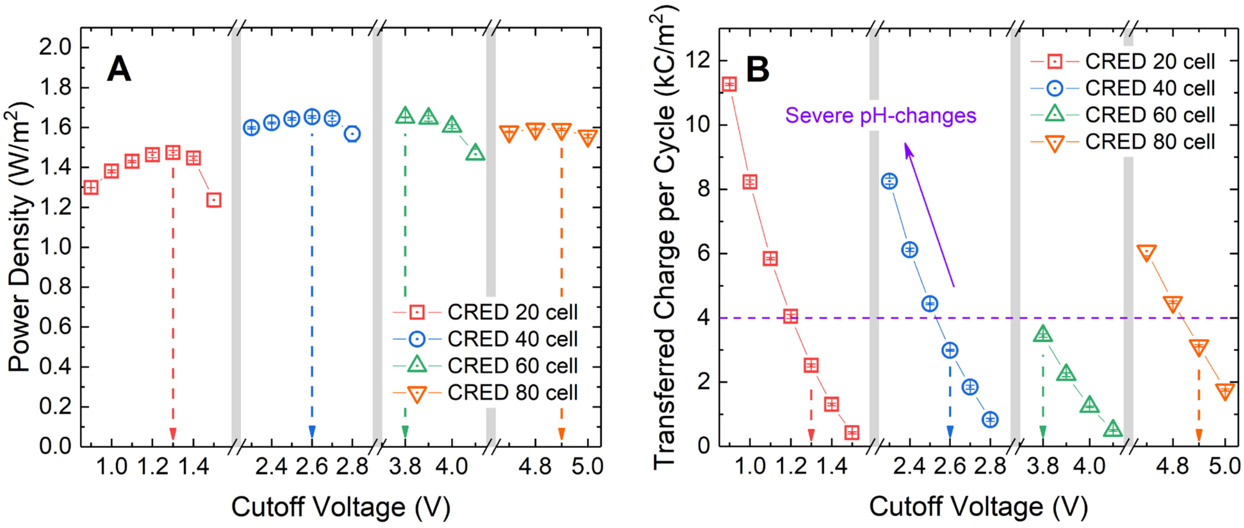

Figure 5. The power density of CRED at different cutoff voltages with different numbers of cell pairs. 18.2, 30.1, 41.8, and 51.9 Ω were connected to the CRED system with 20, 40, 60, and 80 cell pairs, respectively (A). The amount of transferred charge and the pH changes at different cutoff voltages for all cell pairs (B). The dashed arrow indicates the cutoff voltage where the maximum power density is obtained. The dashed line indicates the amount of transferred charge per cycle where the pH changes starts.

CRED Performance *vs.* RED Performance. Figure 6 shows the maximum power density of the bench-scale CRED and RED systems. The lower power density at 20 cell pairs is likely due to the electrical resistance of the electrode system. Considering the electrical resistance of the electrode system is constant, the power consumption by the electrode system may constrain the overall power density with a small number of cell pairs. When increasing the number of cell pairs, this power consumption becomes insignificant. The maximum power densities obtained from CRED are only 1% lower than those from the conventional RED for 60 and 80 cell pairs. Not only were the maximum power densities obtained at very high operating voltages, but they were also obtained without irreversible faradaic reactions. The maximum power density of approximately 1.6 W m^{-2} is much higher than any reported CapMix processes (*i.e.*, 0.007 – 0.2 W m^{-2})[17–19,30,31] and even almost doubled compared to CRED in the previous study (*i.e.*, 0.95 W m^{-2}).[20]

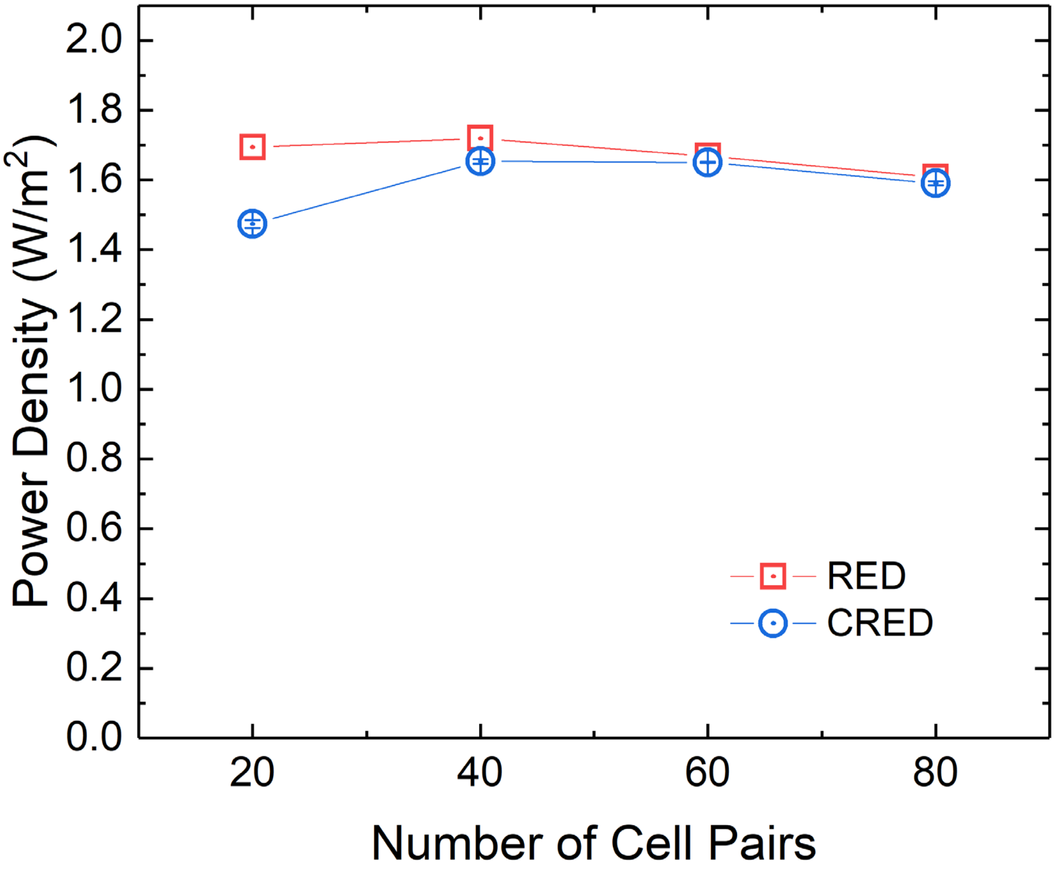

Figure 6. Comparison of the maximum power density of the bench-scale CRED and RED systems with different numbers of cell pairs.

It is instructive to note that the main driving force for both RED and CRED systems is the Donnan potential that is generated by salinity gradients across IEMs. However, the Ohmic resistance of the CRED electrode pair weighs against the charge transfer resistance (*i.e.*, overpotential according to the Butler-Volmer eq.) of quasi-reversible redox couples. In this study, the Ohmic resistance of the CRED electrode pair is still higher; therefore, for the efficient conversion from the chemical potential to power, engineered electrodes are needed.

Recent studies[24,32] demonstrated that the electrode potential could be combined with the Donnan potential in a concentration flow cell, resulting in improved power density. In those studies, a single IEM and a pair of redox (average power density = 3.8 W m^{-2})[24] or capacitive electrodes (average power density = 0.95 W m^{-2})[32] was used to maximize the potentials from synthetic seawater (0.513 M NaCl) and freshwater (0.017 M NaCl). However, when stacking IEMs between the electrodes, which is a typical RED configuration, the influence of the electrode potential would be diminished as the number of cell pairs increases. Thereby, the Donnan potential predominates the overall voltage and power density of the concentration flow cell, which means the performance would not be different from a conventional RED.

Although a CRED stack cannot easily surpass the power density of a conventional RED stack with a reversible redox couple, the main gain for capacitive electrodes is to be achieved in the elimination of potentially irreversible or dangerous faradaic reactions. A large-scale RED suffers from undesired results, including fouling and performance decline by irreversible faradaic reactions at a high stack voltage, as evidenced by the previous studies.[12,15] The current study shows that the CRED system can potentially sustain and stabilize power generation without pH changes, even at high operating voltages.

ASSOCIATED CONTENT

The Supporting Information is available free of charge at xxxx.

Supporting information

A bench-scale CRED system **(Figure S1),** the power density of the conventional RED system co obtained from linear sweep voltammetry (LSV), constant current, chronopotentiometry, constant load discharge, and the maximum power density (D) (**Figure S2),** SEM images of the AC electrode (**Figure S3**), adsorption and desorption isotherms of the AC electrode (**Figure S4)**, the water contact angle on the AC electrode surfaces with time (**Figure S5**), the detailed power profile of the CRED system with 20 cell pairs connected to an external resistor (**Figure S6**), external resistance and corresponding operating voltage result in the maximum power density of the conventional RED system at different numbers of cell pairs (**Table S1**).

AUTHOR INFORMATION

Corresponding Authors

Jin-Soo Park – Department of Green Chemical Engineering, College of Engineering, Sangmyung University, 31 Sangmyungdae-gil, Dongnam-gu, Cheonan-si, Chungnam Province 31066, Republic of Korea; orcid.org/0000-0003-4487-946X; Email: energy@smu.ac.kr

Soryong Chae – Department of Chemical and Environmental Engineering, University of Cincinnati, Cincinnati, Ohio 45221, United States; orcid.org/0000-0002-2382-4075; Email: chaesg@ucmail.uc.edu

Authors

Yoontaek Oh – Department of Chemical and Environmental Engineering, University of Cincinnati, Cincinnati, Ohio 45221, United States; orcid.org/0000-0002-7413-1033

Ji-hyung Han – Jeju Global Research Center, Korea Institute of Energy Research, Jeju-si, Jeju Province 63357, Republic of Korea; orcid.org/0000-0001-7577-392X

Han-ki Kim – Jeju Global Research Center, Korea Institute of Energy Research, Jeju-si, Jeju Province 63357, Republic of Korea; /orcid.org/0000-0002-0184-7356

Namjo Jeong – Jeju Global Research Center, Korea Institute of Energy Research, Jeju-si, Jeju Province 63357, Republic of Korea

David A. Vermaas – Department of Chemical Engineering, Faculty of Applied Sciences, Delft University of Technology, Netherlands; orcid.org/0000-0002-4705-6453

Notes The authors declare no competing financial interest.

ACKNOWLEDGMENTS

This work was conducted under the framework of the Research and Development Program of the Korea Institute of Energy Research (KIER) (Project Number: B8-2441).

REFERENCES

(1) Pattle, R. E. Production of Electric Power by Mixing Fresh and Salt Water in the Hydroelectric Pile. *Nature* **1954**, *174*, 660. https://doi.org/10.1038/174660a0.

(2) Post, J. W.; Veerman, J.; Hamelers, H. V. M.; Euverink, G. J. W.; Metz, S. J.; Nymeijer, K.; Buisman, C. J. N. Salinity-Gradient Power: Evaluation of Pressure-Retarded Osmosis and Reverse Electrodialysis. *J. Memb. Sci.* **2007**, *288* (1–2), 218–230. https://doi.org/10.1016/j.memsci.2006.11.018.

(3) Post, J. W.; Hamelers, H. V. M.; Buisman, C. J. N. Energy Recovery from Controlled Mixing Salt and Fresh Water with a Reverse Electrodialysis System. *Environ. Sci. Technol.* **2008**, *42* (15), 5785–5790. https://doi.org/10.1021/es8004317.

(4) Veerman, J.; Saakes, M.; Metz, S. J.; Harmsen, G. J. Reverse Electrodialysis: Evaluation of Suitable Electrode Systems. *J. Appl. Electrochem.* **2010**, *40* (8), 1461–1474. https://doi.org/10.1007/s10800-010-0124-8.

(5) Scialdone, O.; Guarisco, C.; Grispo, S.; Angelo, A. D.; Galia, A. Investigation of Electrode Material - Redox Couple Systems for Reverse Electrodialysis Processes. Part I: Iron Redox Couples. *J. Electroanal. Chem.* **2012**, *681*, 66–75. https://doi.org/10.1016/j.jelechem.2012.05.017.

(6) Scialdone, O.; Albanese, A.; D’Angelo, A.; Galia, A.; Guarisco, C. Investigation of Electrode Material - Redox Couple Systems for Reverse Electrodialysis Processes. Part II: Experiments in a Stack with 10-50 Cell Pairs. *J. Electroanal. Chem.* **2013**, *704*, 1–9.

https://doi.org/10.1016/j.jelechem.2013.06.001.

(7) Lee, S. Y.; Jeong, Y. J.; Chae, S. R.; Yeon, K. H.; Lee, Y.; Kim, C. S.; Jeong, N. J.; Park, J. S. Porous Carbon-Coated Graphite Electrodes for Energy Production from Salinity Gradient Using Reverse Electrodialysis. *J. Phys. Chem. Solids* **2016**, *91*, 34–40. https://doi.org/10.1016/j.jpcs.2015.12.006.

(8) Weinstein, J. N.; Leitz, F. B. Electric Power from Differences in Salinity: The Dialytic Battery. *Science* **1976**, *191* (4227), 557–559. https://doi.org/10.1126/science.191.4227.557.

(9) Jagur-Grodzinskr, J.; Kramer, R. Novel Process for Direct Conversion of Free Energy of Mixing into Electric Power. *Ind. Eng. Chem. Process Des. Dev.* **1986**, *25* (2), 443–449. https://doi.org/10.1021/i200033a016.

(10) Turek, M.; Bandura, B. Renewable Energy by Reverse Electrodialysis. *Desalination* **2007**, *205* (1–3), 67–74. https://doi.org/10.1016/j.desal.2006.04.041.

(11) D'Angelo, A.; Tedesco, M.; Cipollina, A.; Galia, A.; Micale, G.; Scialdone, O. Reverse Electrodialysis Performed at Pilot Plant Scale: Evaluation of Redox Processes and Simultaneous Generation of Electric Energy and Treatment of Wastewater. *Water Res.* **2017**, *125*, 123–131. https://doi.org/10.1016/j.watres.2017.08.008.

(12) Han, J. H.; Hwang, K. sik; Jeong, H.; Byeon, S. Y.; Nam, J. Y.; Kim, C. S.; Kim, H.; Yang, S. C.; Choi, J. Y.; Jeong, N. Electrode System for Large-Scale Reverse Electrodialysis: Water Electrolysis, Bubble Resistance, and Inorganic Scaling. *J. Appl. Electrochem.* **2019**, *49* (5), 517–528. https://doi.org/10.1007/s10800-019-01303-4.

(13) Liu, F.; Coronell, O.; Call, D. F. Electricity Generation Using Continuously Recirculated Flow Electrodes in Reverse Electrodialysis. *J. Power Sources* **2017**, *355*, 206–210. https://doi.org/10.1016/j.jpowsour.2017.04.061.

(14) Tedesco, M.; Scalici, C.; Vaccari, D.; Cipollina, A.; Tamburini, A.; Micale, G. Performance of the First Reverse Electrodialysis Pilot Plant for Power Production from Saline Waters and Concentrated Brines. *J. Memb. Sci.* **2016**, *500*, 33–45.

https://doi.org/10.1016/j.memsci.2015.10.057.

(15) Nam, J. Y.; Hwang, K. S.; Kim, H. C.; Jeong, H.; Kim, H.; Jwa, E.; Yang, S. C.; Choi, J.; Kim, C. S.; Han, J. H.; Jeong, N. Assessing the Behavior of the Feed-Water Constituents of a Pilot-Scale 1000-Cell-Pair Reverse Electrodialysis with Seawater and Municipal Wastewater Effluent. *Water Res.* **2019**, *148*, 261–271. https://doi.org/10.1016/j.watres.2018.10.054.

(16) Brogioli, D. Extracting Renewable Energy from a Salinity Difference Using a Capacitor. *Phys. Rev. Lett.* **2009**, *103* (5), 058501. https://doi.org/10.1103/PhysRevLett.103.058501.

(17) Brogioli, D.; Zhao, R.; Biesheuvel, P. M. A Prototype Cell for Extracting Energy from a Water Salinity Difference by Means of Double Layer Expansion in Nanoporous Carbon Electrodes. *Energy Environ. Sci.* **2011**, *4* (3), 772–777. https://doi.org/10.1039/c0ee00524j.

(18) Sales, B. B.; Saakes, M.; Post, J. W.; Buisman, C. J. N.; Biesheuvel, P. M.; Hamelers, H. V. M. Direct Power Production from a Water Salinity Difference in a Membrane-Modified Supercapacitor Flow Cell. *Environ. Sci. Technol.* **2010**, *44* (14), 5661–5665. https://doi.org/10.1021/es100852a.

(19) Liu, F.; Schaetzle, O.; Sales, B. B.; Saakes, M.; Buisman, C. J. N.; Hamelers, H. V. M. Effect of Additional Charging and Current Density on the Performance of Capacitive Energy Extraction Based on Donnan Potential. *Energy Environ. Sci.* **2012**, *5* (9), 8642–8650. https://doi.org/10.1039/c2ee21548a.

(20) Vermaas, D. A.; Bajracharya, S.; Sales, B. B.; Saakes, M.; Hamelers, B.; Nijmeijer, K. Clean Energy Generation Using Capacitive Electrodes in Reverse Electrodialysis. *Energy Environ. Sci.* **2013**, *6* (2), 643–651. https://doi.org/10.1039/c2ee23562e.

(21) Campione, A.; Cipollina, A.; Toet, E.; Gurreri, L.; Bogle, I. D. L.; Micale, G. Water Desalination by Capacitive Electrodialysis: Experiments and Modelling. *Desalination* **2020**, *473*, 114150. https://doi.org/10.1016/j.desal.2019.114150.

(22) USGS Current Conditions for USGS 07374000 Mississippi River at Baton Rouge, LA https://waterdata.usgs.gov/usa/nwis/uv?site_no=07374000.

(23) Oh, Y.; Jeong, Y.; Han, S. J.; Kim, C. S.; Kim, H.; Han, J. H.; Hwang, K. S.; Jeong, N.; Park, J. S.; Chae, S. Effects of Divalent Cations on Electrical Membrane Resistance in Reverse Electrodialysis for Salinity Power Generation. *Ind. Eng. Chem. Res.* **2018**, *57* (46), 15803–15810. https://doi.org/10.1021/acs.iecr.8b03513.

(24) Kim, T.; Logan, B. E.; Gorski, C. A. High Power Densities Created from Salinity Differences by Combining Electrode and Donnan Potentials in a Concentration Flow Cell. *Energy Environ. Sci.* **2017**, *10* (4), 1003–1012. https://doi.org/10.1039/c7ee00188f.

(25) Kim, T.; Yu, J.; Kim, C.; Yoon, J. Hydrogen Peroxide Generation in Flow-Mode Capacitive Deionization. *J. Electroanal. Chem.* **2016**, *776*, 101–104. https://doi.org/10.1016/j.jelechem.2016.07.001.

(26) He, D.; Wong, C. E.; Tang, W.; Kovalsky, P.; David Waite, T. Faradaic Reactions in Water Desalination by Batch-Mode Capacitive Deionization. *Environ. Sci. Technol. Lett.* **2016**, *3* (5), 222–226. https://doi.org/10.1021/acs.estlett.6b00124.

(27) Dykstra, J. E.; Keesman, K. J.; Biesheuvel, P. M.; van der Wal, A. Theory of PH Changes in Water Desalination by Capacitive Deionization. *Water Res.* **2017**, *119*, 178–186. https://doi.org/10.1016/j.watres.2017.04.039.

(28) Zhang, C.; He, D.; Ma, J.; Tang, W.; Waite, T. D. Faradaic Reactions in Capacitive Deionization (CDI) - Problems and Possibilities: A Review. *Water Res.* **2018**, *128*, 314–330. https://doi.org/10.1016/j.watres.2017.10.024.

(29) Liu, F.; Coronell, O.; Call, D. F. Effect of Cross-Chamber Flow Electrode Recirculation on PH and Faradaic Reactions in Capacitive Deionization. *Desalination* **2020**, *492*, 114600. https://doi.org/10.1016/j.desal.2020.114600.

(30) La Mantia, F.; Pasta, M.; Deshazer, H. D.; Logan, B. E.; Cui, Y. Batteries for Efficient Energy Extraction from a Water Salinity Difference. *Nano Lett.* **2011**, *11* (4), 1810–1813. https://doi.org/10.1021/nl200500s.

(31) Ye, M.; Pasta, M.; Xie, X.; Dubrawski, K. L.; Xu, J.; Liu, C.; Cui, Y.; Criddle, C. S. Charge-Free

Mixing Entropy Battery Enabled by Low-Cost Electrode Materials. *ACS Omega* **2019**, *4* (7), 11785–11790. https://doi.org/10.1021/acsomega.9b00863.

(32) Zhu, H.; Xu, W.; Tan, G.; Whiddon, E.; Wang, Y.; Arges, C. G.; Zhu, X. Carbonized Peat Moss Electrodes for Efficient Salinity Gradient Energy Recovery in a Capacitive Concentration Flow Cell. *Electrochim. Acta* **2019**, *294*, 240–248. https://doi.org/10.1016/j.electacta.2018.10.053.